Synthesis of oxide nanotubes on Ti13Nb13Zr alloy by the electrochemical method

Piotr Handzlik[1] · Kamil Gutkowski[1]

Abstract

Surface modification of titanium alloys expands the range of their applicability in medicine, particularly in the form of various implants. Present work reports the results of the electrochemical formation of self-ordered oxide nanotubes on Ti13Nb13Zr alloy. Due to its relatively low Young modulus (77–79 GPa) this alloy can be attractive material for orthopedic application. The experiments were conducted in the $(NH_4)_2SO_4 + NH_4F$ electrolyte at room temperature. Anodization of the alloy samples was carried out for 2 h under variable external potential U (in the range from 10 to 45 V) and the current versus time transients were recorded. Obtained surface morphology was investigated by the scanning electron microscopy and the X-ray techniques. The morphological parameters of the obtained nanotubes such as the inner (d_{in}) and outer (d_{out}) diameters were determined. The tubes diameter dependence on the voltage of anodization process was derived. The dependence d[nm] = f(U) [V] was established at constant temperature 25 °C. It provides the basis for controlled oxide nanotubes layer growth. It was also demonstrated that these nanotubes exhibit photocatalytic activity.

Keywords Ti13Nb13Zr alloy · Nanotubes · Anodic oxidation

1 Introduction

During oxidation of a number of metals, the formation of one-dimensional nanostructure of the oxide layer having the shape of nanotubes has been observed. These self-organized structures having well developed surfaces and high specific surface area attracted a lot of attention as potential materials used in photocatalysis [1], solar cells [2] sensors [3], hydrogen generation [4], wastewater treatment [5] and (perhaps most important) in biomedical field [6, 7]. It was found that titanium and its alloys can be appropriate implant materials, which can be used as orthopedic and dental implants as well as blood clotting agents [8]. Oxide nanotubes formation on Ti can be obtained in the course of the electrochemical anodization process during which the size and shape of nanotubular arrays may be controlled to a large extend. However, during biomedical applications at least three problems must be taken into account.

First, and probably the most important, is connected with the biomechanical properties of the metal. The elastic modulus for Ti is about 100 GPa, while that of the human bones may vary (depending on the bone) between 2 and 30 GPa. This problem can be somehow avoided by the addition of alloying elements to titanium, which may decrease the elastic modulus of the alloy. The best result so far has been achieved by preparing the alloy Ti24Nb4Zr7.9Sn which exhibits elastic modulus equal to 46 GPa [9]. The second problem is connected with the alloying element itself. It must be non-toxic. Thus, a number of potentially interesting elements from the point of view of biomechanical properties must be excluded since they transfer through the oxide layer into the human body may bring about unwanted and harmful effects. Needless to say, the corrosion process of the alloy in the environment of the body fluids must be known. Finally, the metallic surface often does not support the osseointegration. Attempts are being made to solve this problem with proper surface treatment and the formation of oxide nanotubular coatings is a possible solution.

Moreover, it is known that to enhance implant's bonding with adjacent bone surface, the formation of hydroxyapatite (HAp) coating is helpful. Hydroxyapatite has the ability to form bond-like layer on the oxide surface, which bonds

✉ Piotr Handzlik
  phandzli@agh.edu.pl

1 Faculty of Non-Ferrous Metals, AGH University of Science and Technology, Cracow, Poland

to the bone. Thus, there is a question how to influence the hydroxyapatite formation. One important factor in HAp formation is the surface area and roughness of the oxide layer. Tsuchiya et al. [10] studied the HAp formation on different TiO_2 nanotube layers in SBF solutions. They confirmed that the presence of nanotubes (NT's) on metal surface enhances the formation of hydroxyapatite layer. The best results were obtained for long nanotubes composed of anatase + rutile mixture. Kim et al. [11] and Oh et al. [6] found that in the presence of NaOH in SBF solution, the exchange between charged Na^+ and Ca^{2+} ions may take place, accelerating HAp formation on the oxide surface.

Detailed study of Kim et al. [12] demonstrated that the overall process of hydroxyapatite formation is composed of three steps. At first, sodium titanate is formed on the surface which next converts into calcium titanate, and finally into apatite with bone like structure. This overall process is accompanied with the surface charge variation. Kar et al. [13] investigated electrodeposition process of HAp onto nanotubular TiO_2. They used two-step process which consisted in potential pulsing followed by constant current flow. They found that hydroxyapatite growth was vertical with increased bond strength of the coating.

These experiments may suggest that by influencing nanotubes reactivity with ions in the solution one may facilitate the process of HAp formation which in all cases had something to do with the charge transfer. Therefore, one can imagine another process making use of opposite charge attraction. It is proved that TiO_2 based nanomaterials exhibit extraordinary catalytic activity under the action of light [14]. Irradiated TiO_2 generates electron–hole pair:

$$TiO_2 + h\nu(UV) = TiO_2(e^-) + TiO_2(h^+) \qquad (1)$$
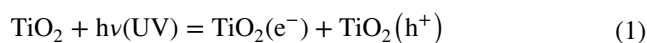
which can be separated in the solution along a long nanotube. Consequently, two sides of the tube should have different charges. It remains to be seen if these charges may react with either Ca^{2+} or $(PO_4)^{2-}$ ions enhancing apatite growth under irradiation.

In our previous work we investigated electrochemical synthesis of oxide nanotubes on Ti6Al7Nb alloy [15]. In that work we demonstrated that the size of nanotubes can be effectively controlled by the anodization potential. In this work, the alloy with even lower elastic modulus (114 vs. about 80 GPa) i.e. Ti13Nb13Zr has been investigated. This alloy was developed by Davidson and Kovacs [16] in 1992, and was found to exhibit excellent biocompatibility. The process of formation of TiO_2 nanotubes on this alloy was investigated by Stróż et al. [17, 18] and Ossowska et al. [19]. Electrochemical corrosion

behaviour in Ringer's solution of nanotubular oxide developed on its surface as well as the influence of the heat treatment was reported by Saji and Choe [20]. Our interest has been focused on the electrochemical control of tubes dimensions. It is known that oxide nanotubes are not easily formed on niobium [21, 22]. Our investigated alloy contains 13 wt% of Nb, thus the aim of the present study is the following:

- first, to find out if increased content of Nb in Ti may affect the process of nanotubes growth rate and their formation
- second, to derive nanotubes diameter versus voltage dependence since it is commonly known that the key factor controlling the tube dimension is the anodization voltage.
- third, to find out if the presence of Nb or Zr oxides in NT's layer may influence its photocatalytic activity, so characteristic for pure TiO_2.

2 Experimental

In this work the Ti13Nb13Zr alloy (ASTM F17130-03, rod ϕ12 mm, Wolften, Poland) of chemical composition as shown in Table 1 was used in the experiments. Ti13Nb13Zr alloy rod was cut into slices on the cutting wheel Struers Secotom 50. Then the slices were mounted into epoxy resin by using PRESI Mecapress 3. They were mechanically grounded and polished on the cloth up to 1 μm, and then ultrasonically cleaned using deionised water and acetone. The samples having area of 0.5 cm^2 were anodized in the electrolyte containing 1 M $(NH_4)_2SO_4$ (POCH) and 0.5 wt% NH_4F (POCH). During all anodization experiments the electrolyte was stirred using mechanical stirrer with rotation speed equal 200 rpm. Electrochemical oxidation was carried out at room temperature in two-electrode electrochemical cell with platinum sheet as counter electrode (CE) and Ti13Nb13Zr alloy as a working electrode (WE). As a power supply, programmable DC Power Supply Agilent N5751A was used. To record the current versus time dependence digital multimeter Rigol DM3064 was used. The electrochemical setup and the anodization procedure were similar to that reported in our previous paper [23]. Anodic oxidation was conducted at a constant potential which varied in the range from 10 to 45 V with step 5 V. After anodization, samples were rinsed with deionised water and ultrasonically cleaned and next dried in air stream. Then the chosen sample anodized at 20 V, was annealed at 450 °C for 3 h to change the structure of nanotubes layer from amorphous to crystalline.

The morphology of the "pure" alloy sample as well as anodized samples was investigated by using field emission

Table 1 Chemical composition of the Ti13Nb13Zr alloy, wt% - manufacturer certificate

Nb	Zr	Fe	C	N	O	H
13.1	13.3	0.1	0.05	0.011	0.08	0.001

scanning electron microscope (FE-SEM) Hitachi SU-70. Chosen samples were studied by point and region analyses using EDS analysis (Thermo Scientific) attached to the SEM to obtain chemical composition of the phases. The point analyses were performed over five points or areas in each phase. Data acquisition and calculations of chemical composition were done by using NSS 3 software. Generally, for each element an error within 0.2 at% was ascribed. After investigation of the microstructure, each sample was subjected to X-ray diffraction (Rigaku Mini Flex II) using monochromatic Cu Kα radiation (0.15416 nm). XRD spectra were solved by using PDXL software (Rigaku, Japan) with ICDD PDF 2 + Release 2010 database. All measurements of nanotubes diameters were performed by using AxioVision v 4.8 software (Zeiss Germany).

The photocatalytic activity of oxides nanotubes layer was investigated by the 3 h degradation of methyl orange solution under UV light irradiation. To perform this experiments sample anodized at 20 V has been chosen. The UV light was provided by the 200 W mercury-xenon lamp (HAMAMATSU Lightningcure Spot light source LC8, Japan) with radiation wavelength of 365 nm. An 0.5 cm^2 (geometrical area) nanotubes layer was immersed into 20 cm^3 of aqueous methyl orange solution with a concentration of 10 mg/dm^3 in the same cell which was used for anodization process. The solution was stirred using magnetic stirrer with rotation speed equal 150 rpm. The sample was left in the cell prior to UV illumination for 30 min in a darkness to achieve adsorption/desorption equilibrium. During the photocatalytic process, the absorbance of the MO solution was recorded every 30 min using an UV–Vis V-770 spectrophotometer (JASCO, Japan) with wavelengths in the 200–800 nm range. The absorption intensities before and after degradation as well as the degradation ratio of MO can be calculated as follows:

$$\frac{C}{C_0} = \frac{A}{A_0} \tag{2}$$

$$D(\%) = \frac{A_0 - A}{A_0} * 100 \tag{3}$$

where D is the degradation ratio, C_0 and A_0 are the concentration and absorbance of the initial MO solution, C and A are the concentration and measured absorption intensity after degradation for a known time.

3 Results and discussion

The microstructure of anodic oxide layer was observed by FE-SEM. Figure 1a–d show SEM images of mixed oxide nanotubes fabricated by anodic oxidation in aqueous solution containing 1 M $(NH_4)_2SO_4$ and 0.5 wt% NH_4F. Anodizing voltage and time were 30 V and 2 h, respectively.

As one can see, highly ordered oxide nanotubes were obtained on the surface of Ti13Nb13Zr alloy. As-formed nanotubes were studied by point and region analyses using EDS technique to obtain their chemical composition. Table 2 presents the chemical composition of 5 selected surface areas of nanotubes which are marked in Fig. 2. The EDS analysis revealed the presence of three constituent elements of the alloy in upper parts of nanotubes, confirming

Fig. 1 SEM images of mixed oxide nanotubes obtained at 30 V: **a** top view, **b** bottom view **c** cross section **d** the Ti13Nb13Zr alloy base
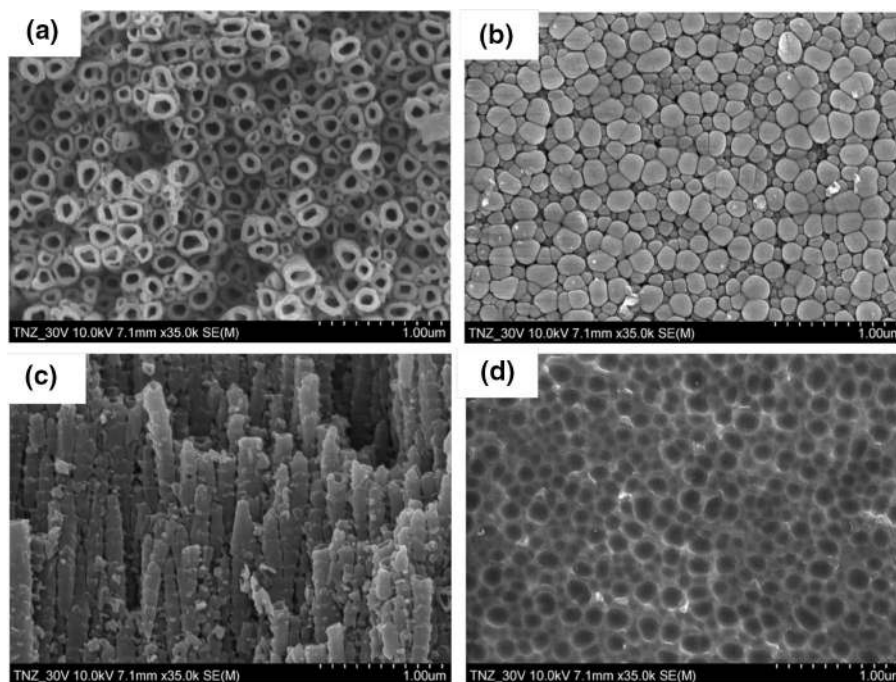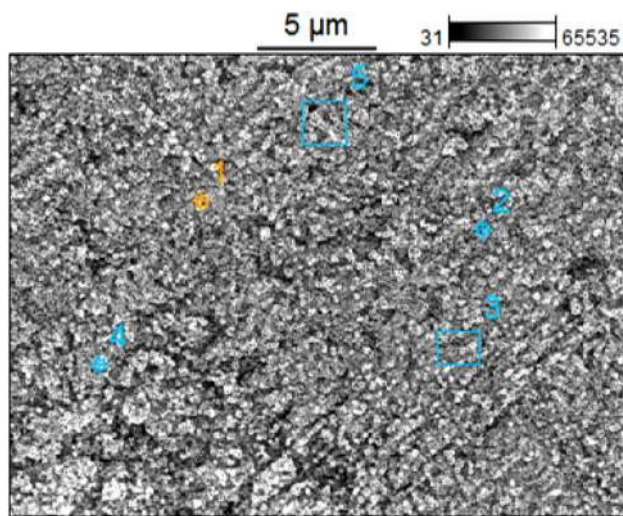
Table 2 The EDS analysis results (wt%) of nanotubes formed at 30 V

Point, region	Ti	Nb	Zr	O	F	Au
1	28.6	4.0	4.2	54.2	7.4	1.6
2	40.9	5.7	5.3	41.5	5.6	1.1
3	35.3	5.0	4.8	47.0	6.6	1.3
4	32.3	4.4	4.8	50.4	6.2	1.9
5	34.1	4.8	4.7	48.7	6.4	1.4
Avg	34.2	4.8	4.8	48.4	6.4	1.4

Fig. 2 Points and regions of analysis marked in SEM image

the presence of niobium and zirconium oxides in synthesized nanotubular layer. It can be believed that the nanotubes formed on Ti13Nb13Zr alloy may possess enhanced mechanical properties and adhesion to substrate [20]. It can be also seen that the nanostructures produced by anodization contain also F⁻ ions which can be removed by thermal treatment at 200 °C [15]. Gold is also present on the surface because it was sprayed onto samples to make SEM observations and chemical analyses possible.

Anodization of the samples was carried out in the voltage range from 10 to 45 V, and nanotubes morphology was obtained in this whole voltage range what is shown in Fig. 3.

In this voltage range, the outer tube diameter varied approximately in the range from 65 to 285 nm, while the inner diameter varied in the range from 29 to 182 nm. In both cases the diameter increases approximately linearly with increasing anodization voltage, but at different rate. The change of nanotubes diameter with anodization voltage is shown in Fig. 4. We found that the increase of the diameters can be described with the following linear equations:

$$d_{inner} = 4.45 \times U(V) - 21.64 \ [nm] \tag{4}$$

$$d_{outer} = 6.35 \times U(V) - 10.08 \ [nm]. \tag{5}$$

The comparison of these equations with the results obtained for Ti6Al7Nb alloy indicates that the oxide layer growth is faster for Ti13Nb13Zr alloy.

During all electrochemical oxidation experiments current as a function of time was recorded. One can observe that the values of current density increase with the increasing anodization voltage values (Fig. 5). The current density versus time curve for electrolyte containing fluorides deviates from the classical high-field growth. After an initial exponential decay (phase I) the current increases again (phase II). Then, the current reaches a quasi-steady state (phase III). Such a current behavior can be related to different stages in the pore formation process. In the first stage, a barrier oxide is formed, leading to a current decay (I). In the next stage, the surface is locally activated and pores start to grow randomly (II). Due to the pore growth the active area increases and the current increases. This leads to a situation, where the pores equally share the available current, and self-ordering under steady state conditions is established (III) [24].

Figure 6 presents the XRD spectra for "pure" alloy as well as for samples which were anodized at chosen voltages and the annealed one. XRD patterns of anodized samples exhibited only the peaks corresponding to the α and β alloy phases, which proves the amorphous nature of the anodically formed nanotubes. To obtain crystalline and more stable nanotubular oxide layer, the heat treatment process is needed. The sample annealed at 450 °C for 3 h contains a pure anatase phase what is in agreement with the fact, that anatase phase appears in the temperature range 300–500 °C (rutile phase dominates in nanotubes annealed at 700 °C) [24].

Figure 7 shows the photodegradation of the methyl orange (MO) solution using the UV irradiation separately and using UV light together with the nanotubes layer as a catalyst. The change of the MO concentration is much faster in the case of photocatalytic process. After 3 h of test, degradation ratio calculated accordingly to Eq. 3 is equal 4.5% for process performed only with UV light and 13.4% for photocatalytic experiment. These results show that mixed oxides nanotubular film can act as a good catalyst for dye degradation processes. Moreover, the good photocatalytic activity of these nanomaterial can be applied in hydroxyapatite formation under light illumination.

Fig. 3 SEM top views of nanotubular oxide layers formed at different voltages during 2 h anodization
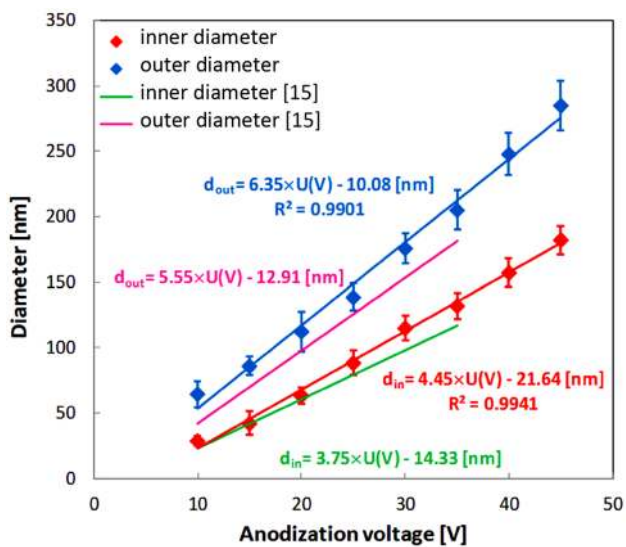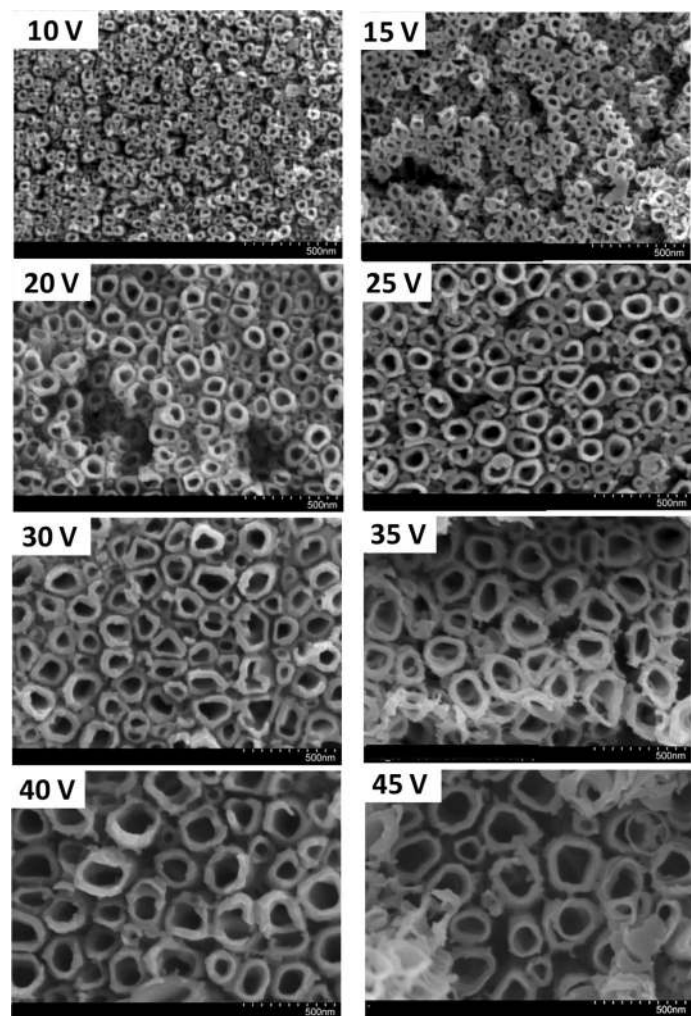

Fig. 4 The change of nanotubes diameters as a function of anodization voltage
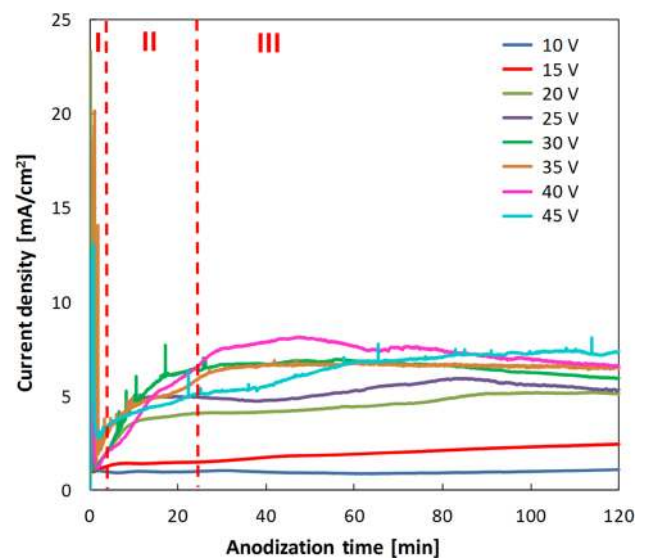
Fig. 5 Current versus time curves recorded during anodization experiments with marked three stages of pores formation process
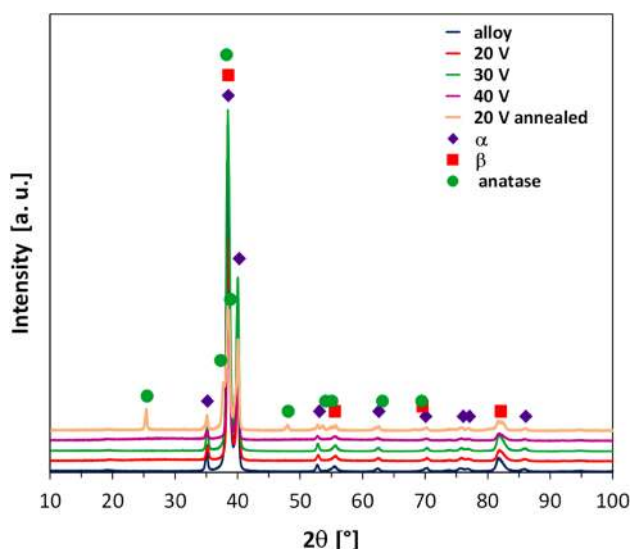
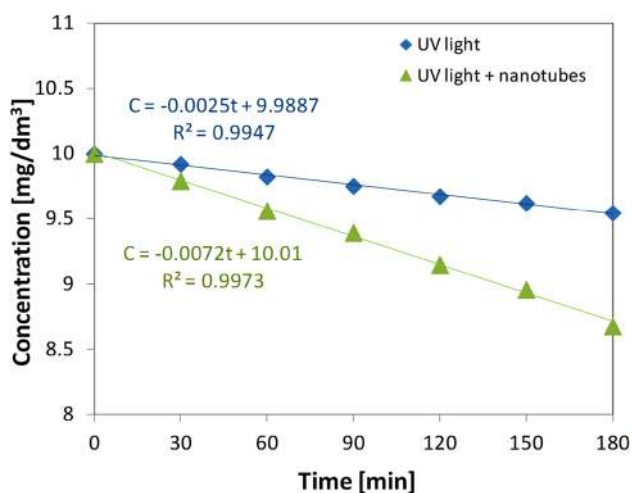**Fig. 6** XRD spectra of Ti13Nb13Zr alloy and nanotubes formed at chosen voltages

Fig. 7 The degradation of methyl orange by photolytic and photocatalytic process

4 Conclusions

The electrochemical oxidation of Ti13Zr13Nb alloy in aqueous electrolyte containing fluoride ions results in a fine nanotubular structure determined by SEM morphology investigations. The nanotubes consist of mixed oxides of alloy components (SEM–EDS) and are found to be amorphous (XRD). It seems, that the best developed nanotubes are obtained for voltages in the range from 20 to 40 V. The increased amount of Nb in the alloy in fact did not affect the tube formation. Its influence had to be compensated by zirconium addition. We found previously that

ZrO_2 nanotubes can be formed easily on zirconium surface [23]. The diameters of synthesized nanotubes depend linearly on applied anodizing voltage in the range from 10 to 45 V. Derived linear dependencies $d = f(U)$ can be used in the future to synthesize nanotubes with expected geometrical dimensions under optimized conditions presented in this work. It was also demonstrated that these nanotubes exhibit photocatalytic activity which can be exploited during hydroxyapatite formation under light illumination.

References

1. L.L. Costa, A.G.S. Prado, J. Photochem. Photobiol., A **201**, 45 (2009)
2. G.K. Mor, O.K. Varghese, M. Paulose, K. Shankar, C.A. Grimes, Sol. Energy Mat. Sol. Cells **90**, 2011 (2006)
3. M.-H. Seo, M. Yuasa, T. Kida, J.-S. Huh, K. Shimanoe, N. Yamazoe, Sensors Actuat. B **137**, 513 (2009)
4. Z. Liu, B. Pesic, K.S. Raja, R.R. Rangaraju, M. Misra, Int. J. Hydrog. Energy **34**, 3250 (2009)
5. M. Tian, S.S. Thind, J.S. Dondapati, X. Li, A. Chen, Chemosphere **209**, 182 (2018)
6. S.-H. Oh, R.R. Finones, C. Daraio, L.-H. Chen, S. Jin, Biomaterials **26**, 4938 (2005)
7. B. Ercan, T.J. Webster, Biomaterials **31**, 3684 (2010)
8. K. Indira, U.K. Mudali, T. Nishimura, N. Rajendran, J. Bio Tribo Corros. **1**, 28 (2015)
9. Y. Li, C. Yang, H. Zhao, S. Qu, X. Li, Y. Li, Materials **7**, 1709 (2014)
10. H. Tsuchiya, J.M. Macak, L. Müller, J. Kunze, F. Müller, P. Greil, S. Virtanen, P. Schmuki, J. Biomed. Mater. Res. **77A**, 534 (2006)
11. H.-M. Kim, F. Miyaji, T. Kokubo, T. Nakamura, J. Biomed. Mater. Res. **32**, 409 (1996)
12. H.-M. Kim, T. Himeno, M. Kawashita, J.-H. Lee, T. Kokubo, T. Nakamura, J. Biomed. Mater. Res. **67A**, 1305 (2003)
13. A. Kar, K.S. Raja, M. Misra, Surf. Coat. Technol. **201**, 3723 (2006)
14. Q. Zhou, Z. Fang, J. Li, M. Wang, Microporous Mesoporous Mater. **202**, 22 (2015)
15. M. Stępień, P. Handzlik, K. Fitzner, J. Solid State Electrochem. **20**, 2651 (2016)
16. J.A. Davidson, P. Kovacs, US Patent 5.169.597, 1992
17. A. Stróż, G. Dercz, B. Chmiela, D. Stróż, B. Łosiewicz, Acta Phys. Pol., A **130**, 1079 (2016)
18. A. Stróż, B. Łosiewicz, M. Zubko, B. Chmiela, K. Balin, G. Dercz, M. Gawlikowski, T. Goryczka, Mater. Charact. **132**, 363 (2017)

19. A. Ossowska, A. Zieliński, M. Supernak, Solid State Phenom. **183**, 137 (2012)
20. V.S. Saji, H.C. Choe, Corros. Sci. **51**, 1658 (2009)
21. I. Sieber, H. Hildebrand, A. Friedrich, P. Schmuki, Electrochem. Commun. **7**, 97 (2005)
22. H. Habazaki, Y. Oikawa, K. Fushimi, Y. Aoki, K. Shimizu, P. Skeldon, G.E. Thompson, Electrochim. Acta **54**, 946 (2009)
23. M. Stępień, P. Handzlik, K. Fitzner, J. Solid State Electr. **18**, 3081 (2014)
24. J.M. Macak, H. Tsuchiya, A. Ghicov, K. Yasuda, R. Hahn, S. Bauer, P. Schmuki, Curr. Opin. Solid State Mater. Sci. **11**, 3 (2007)